Computers and Concrete, Vol. 7, No. 4 (2010) 303-315

DOI: http://dx.doi.org/10.12989/cac.2010.7.4.303

Stress resultant model for ultimate load design of reinforced-concrete frames: combined axial force and bending moment

Ba-Hung Pham*[1], Luc Davenne[1], Delphine Brancherie[2] and Adnan Ibrahimbegovic[1]

[1]*École Normale Supérieure de Cachan - Laboratoire de Mécanique et Technologie 61, av. du président Wilson, 94235 Cachan cédex, France*
[2]*Université de Technologie de Compiègne - Laboratoire Roberval BP 20529, 60205 Compiègne Cedex, France*

(Received July 30, 2009, Accepted December 23, 2009)

Abstract. In this paper, we present a new finite Timoshenko beam element with a model for ultimate load computation of reinforced concrete frames. The proposed model combines the descriptions of the diffuse plastic failure in the beam-column followed by the creation of plastic hinges due to the failure or collapse of the concrete and or the re-bars. A modified multi-scale analysis is performed in order to identify the parameters for stress-resultant-based macro model, which is used to described the behavior of the Timoshenko beam element. The micro-scale is described by using the multi-fiber elements with embedded strain discontinuities in mode 1, which would typically be triggered by bending failure mode. A special attention is paid to the influence of the axial force on the bending moment - rotation response, especially for the columns behavior computation.

Keywords: reinforced concrete frames; macro model; embedded discontinuities.

1. Introduction

The standard design procedure of reinforced concrete frame structures starts with linear analysis to obtain the corresponding diagrams of stress resultants (bending moment, shear and axial force), followed by the ultimate analysis of each cross section. The main disadvantage of such a design procedure concerns the (highly) statically indeterminate frames, where the failure of each beam or column would not imply the complete failure of the structure, but would lead to a significant stress resultant redistribution with respect to the result obtained by linear analysis.

The alternative is the performance based design procedure where the behavior until complete failure of beam-column and frames imposes to consider so-called plastic hinges corresponding to the zones where plasticity and/ or damage localizes. Engineering structures are usually statically indeterminate, so that the total failure of one member would affect the global response of the structure but it would not lead to a complete loss of the structural integrity. Moreover, being capable of describing the softening response of the members of one particular structure can provide an estimate of the residual life of a partially damaged structure. Such a procedure can also help to provide a more detailed crack description, which is needed to make decisions about the maintenance

* Corresponding author, Dr. Ba-Hung Pham, E-mail: luc.davenne@lmt.ens-cachan.fr

and repairs.

In that spirit, the Eurocode 2 allows to use a concrete behavior law with a beginning of softening branch instead of the classical parabolic-rectangle without softening curve. But it doesn't warn to the use of softening laws in finite element method, where localizations of strain can prevent the objectivity of the result.

A lot of research works are concerned by the problem of computation with plastic hinges appearance in the reinforced-concrete frame structures (see for example recent papers (Anthoine *et al.* 1997, Cipollina *et al.* 1995, Florez-Lopez 1998, Marante *et al.* 2004, Marante and Florez-Lopez 2003, Rajasankar *et al.* 2009). Many works focus on the evaluation of the ultimate load but only a few works are concerned by the evaluation of the residual life, especially for reinforced concrete beam. Some authors study the softening in plastic hinges (Armero and Ehrlich 2006, Ehrlich and Armero 2005, Jirasek 1997, Nanakorn 2004) and sometimes especially in presence of axial force (Zingales and Elishako 2000).

We developed a stress-resultant marco model for reinforced concrete beams and columns (Pham 2009). This model is a Timoshenko beam element with an embedded rotation discontinuity in its middle. A continuous moment curvature hardening behavior law is used in the regular part overall the element and a singular softening moment rotation law is used on the discontinuity. Treated in the incompatible mode framework, this finite energy approach avoids the localization problems encountered when dealing with softening behavior laws. The parameters of the stress resultant macro model are identified from computations at a more detailed level with multi-fiber beam elements, especially developed for that, where an enhancement is introduced in the fibers to model the softening of materials (concrete and steel).

In Section 2, we present the new Timoshenko beam element. In Section 3, we present the identification procedure, taking into account the coupling between axial force and bending moment. Finally, in Section 4, we present several examples to show the precision and the robustness of the macro-element.

2. Timoshenko beam element with embedded rotation discontinuity

In a Timoshenko beam finite element of length l^e, the classical displacement field, based on linear interpolation functions $N_1(x) = 1 - \frac{x}{l^e}$ and $N_2(x) = \frac{x}{l^e}$, is written as

$$\mathbf{d} = \mathbf{N}\mathbf{D} \tag{1}$$

where

$$\begin{aligned} \mathbf{d}^T &= [u(x)\ v(x)\ \theta(x)] \\ \mathbf{D}^T &= [U_1 V_1 \theta_1 U_2 V_2 \theta_2] \end{aligned} \tag{2}$$

and

$$\mathbf{N} = (\mathbf{N}_1,\ \mathbf{N}_2);\ \text{with}\ \mathbf{N}_i = \begin{bmatrix} N_i & 0 & 0 \\ 0 & N_i & 0 \\ 0 & 0 & N_i \end{bmatrix} \tag{3}$$

$u(x)$ and $v(x)$ are the axial and transversal displacements of the mean line of the beam element and $\theta(x)$ the rotation of its cross sections. U_i V_i and θ_i are the nodal displacements. With the purpose of embedding the rotation discontinuity, the incompatible mode method (Ibrahimbegovic 2009, Ibrahimbegovic and Wilson 1991) is used to enrich the classical rotational displacement interpolation with a jump of rotation α. The rotation can thus be re-written as

$$\theta(x) = N_1(x)\theta_1 + N_2(x)\theta_2 + N_3(x)\alpha \tag{4}$$

with

$$N_3(x) = H_\Gamma(x-x_C) - N_2(x) \tag{5}$$

$H\Gamma$ is the Heanside function and x_c the position of the discontinuity, the middle of the element in our case (see Fig. 1D).

In the spirit of incompatible mode method, (see Ibrahimbegovic 2009, Ibrahimbegovic and Brancherie 2003, Ibrahimbegovic and Wilson 1991), the added part $N_3(x)\alpha$ is used only for the construction of enrichment in the curvature interpolation. The generalized strain $\varepsilon^T=[\varepsilon\,\gamma\,\kappa]$ is written as

$$\varepsilon = \mathbf{BD} + \mathbf{G}\alpha \tag{6}$$

where $\mathbf{B}$ is the derivative interpolation

$$\mathbf{B} = (\mathbf{B}_1, \mathbf{B}_2);\ \text{with}\ \mathbf{B}_i = \begin{bmatrix} \frac{dN_i}{dx} & 0 & 0 \\ 0 & \frac{dN_i}{dx} & -N_i \\ 0 & 0 & \frac{dN_i}{dx} \end{bmatrix} \tag{7}$$

and $\mathbf{G}$ the enhanced interpolation of bending strain, which can also be decomposed into a regular part and a singular part, $\mathbf{G} = \overline{\mathbf{G}} + \overline{\overline{\mathbf{G}}}$

$$\overline{\mathbf{G}} = \begin{bmatrix} 0 \\ 0 \\ -\frac{1}{l^e} \end{bmatrix}\ \overline{\overline{\mathbf{G}}} = \begin{bmatrix} 0 \\ 0 \\ 1 \end{bmatrix}\delta_{x_c} \tag{8}$$

δ_{x_c} is the Dirach function centered at the discontinuity point. We can note that with this choice for the enrichment, the patch test $\int_0^{l^e} \mathbf{G}dx = 0$ is verified. We can thus keep exactly the same

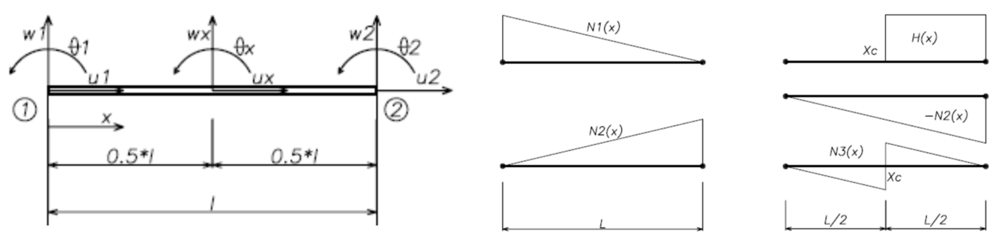

Fig. 1 2D bar element and shapes of the interpolation functions approximation for the virtual strain field as the one use in Eq. (6) for real strain. The stress field approximation over the element can be obtained from the real strain field in Eq. (6) with no contribution from the singular part which is treated alone apart. This stress field $\sigma^T = [N\ V\ M]$ (N axial force, V shear force and M bending moment) is non linear with a constitutive equation of the form

$$\dot{\sigma} = D^{in}\dot{\bar{\varepsilon}} = D^{in}(\mathbf{B}\dot{\mathbf{D}} + \overline{\mathbf{G}}\dot{\alpha}) \tag{9}$$

and the moment-rotation jump relation can be written as

$$\dot{M}_{x_c} = K_{x_c}\dot{\alpha} \tag{10}$$

By exploiting the approximations for virtual strain strains and stresses, the weak form of equilibrium equations can be recast in the format typical of incompatible mode method (A is the finite element assembly procedure)

$$\begin{aligned} &A_{e=1}^{nel} = [f^{int(e)} - f^{ext(e)}] = 0; f^{int(e)} = \int_0^{l^e} \mathbf{B}^T \sigma dx \\ &h^e = 0;\ \forall e \in [1, nel];\ h^e = \int_0^{l^e} \mathbf{B}^T \sigma dx + M_{x_c} \end{aligned} \tag{11}$$

The system of Eq. (11) can be writtem in the incremental form

$$\begin{aligned} &A_{e=1}^{nel} = [K^e \Delta d + F^e \Delta\alpha - f^{ext(e)}] = 0;\ \text{and} \\ &F^{eT}\Delta d + H^e \Delta\alpha + K_{x_c}\Delta\alpha = 0\ \forall e \in [1, nel] \end{aligned} \tag{12}$$

where

$$K^e = \int_0^{l^e} \mathbf{B}^T D^{in} \mathbf{B} dx;\ F^e = \int_0^{l^e} \mathbf{B}^T D^{in} \overline{\mathbf{G}} dx;\ H^e = \int_0^{l^e} \overline{\mathbf{G}}^T D^{in} \overline{\mathbf{G}} dx \tag{13}$$

This set of equations is solved by using the operator split method, (see Ibrahimbegovic 2009). Namely, we first solve local equation in each localized element for a fixed value of total displacement d, so that we can determine the value of the rotation jump α. Then by static condensation at the element level, the first equation in Eq. (12) turns into

$$A_{e=1}^{nel} = [\hat{K}^e \Delta d - f^{ext(e)}] = 0;\ \text{with}\ \hat{K}^e = K^e - F^e (H^e + K_{x_c})^{-1} F^{eT} \tag{14}$$

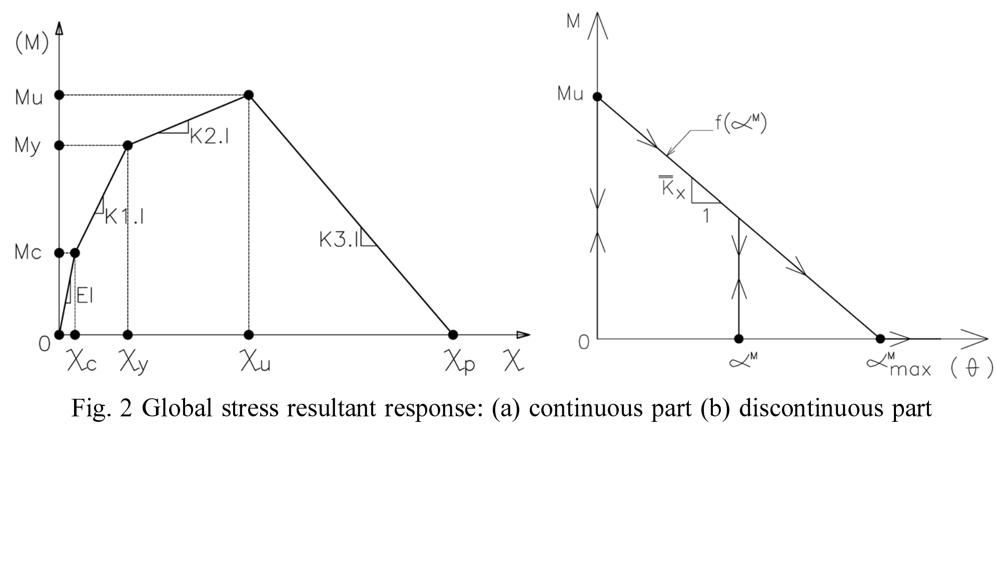

Fig. 2 Global stress resultant response: (a) continuous part (b) discontinuous part

It is important to note that the non linear response is split into two parts:

- a continuous part with diffuse non linearity in the whole element, written with a stress-curvature relationship (Eq. 9). We adopt here a stress-resultant elasto-plastic model with two linear hardening phases (see Fig. 2(a)).
- a discrete part at the discontinuity point, written with a stress-rotation relationship. We adopt here a rigid-plastic model with linear softening (see Fig. 2(b)).

In a such way, we avoid the non objectivity of the response due to strain localization since the plastic hinge dissipates a finite energy. We have also a direct access to the crack opening and do not need post analysis like in Dufour *et al.* (2008). Note that this method is of E-FEM kind, close in ideas to the X-FEM methods (Asferg *et al.* 2007), but different in computational implementation. The area under the curve on Fig. 2(b) is directly related to the fracture energy of the material. For each hardening or softening branch, the threshold function is written as

$$\Phi^M(M, \zeta_i^M) := |M| - (M_i + K_i I \cdot \zeta_i^M) \leq 0 \tag{15}$$

where M_i represents M_c the cracking moment, M_y the yield moment or M_u the ultimate moment. I denotes the cross-section inertia and K_i denotes the different hardening/softening moduli.

In the next section, a method for obtaining the values M_i, K_i and K_{x_c} will be described.

3. Stress resultant model parameter identification

In order to identify the parameters of the stress resultant model presented in section 2, we use a multi-layer Timoshenko beam element described in section 3.1. We use only one element embedded at its left end and loaded while imposing a rotation at its right end (see Fig. 3(b)). We can either impose only a rotation for the beams (Fig. 3(a)) or add an axial force for the columns (Fig. 3(b)). The identification procedure is described in section 3.2.

3.1 Multifiber beam model with embedded discontinuities in fibers

In this section we present shortly the multi fibers beam model which provides the basis for identifying the parameters of stress resultant model. This multi-fiber model is helpful to analyse and handle a beam-column with multi materials embedded in one cross-section in general or for reinforced concrete in particular. For the global coherence of the method, we also use embedded strain discontinuity in each fibers.

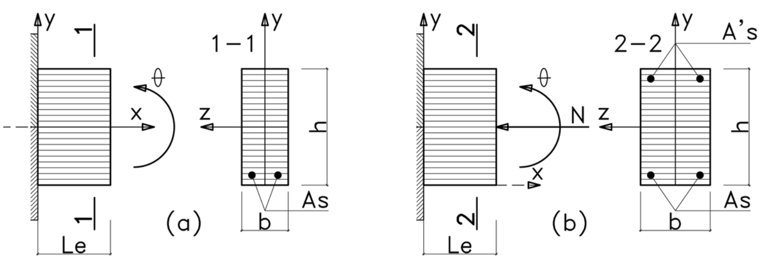

Fig. 3 Multi-fiber elements to compute stress resultant parameters for the macro model

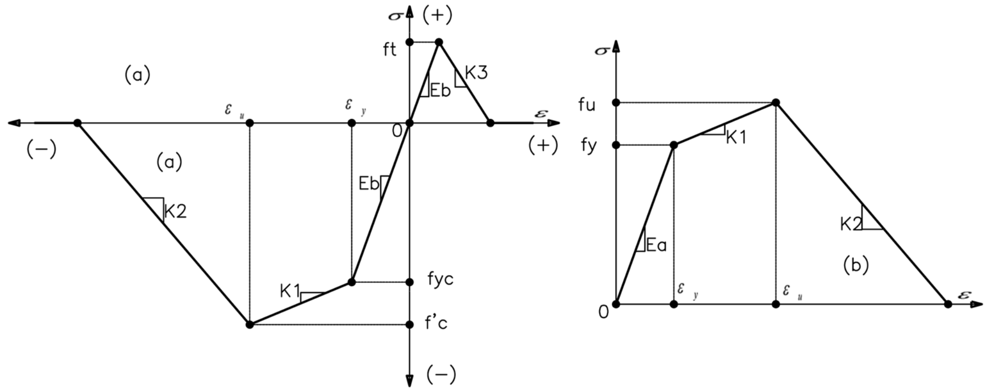

Fig. 4 Behaviors of concrete and steel

Assuming the cross sections remain plane and a uniform repartition of shear strain, the axial and shear strains of each layer can be computed from the element displacements and the position y_i of the layer in the cross section

$$\varepsilon_x^i(x) = \frac{du(x)}{dx} - y_i \frac{d\theta(x)}{dx};\; 2\varepsilon_{xy}^i = \frac{dv(x)}{dx} - \theta(x) \tag{16}$$

In order to be able to represent the strain localization due to the softening of the materials, we folow the same developments as in section 2 in the frame of incompatible modes method. We can introduce an axial strain discontinuity in each fiber, split in a regular part and a singular part

$$\varepsilon_x^i = \bar{\varepsilon}_x^i + \alpha^i \delta_{x_c}^i \tag{17}$$

In a same manner, the axial stress along the fiber depends on the regular strain (stress-strain relationship) and the localized traction on the crack discontinuity in the middle of the fiber depends on the jump of displacement (stress-displacement relationship).

The constitutive laws of concrete and steel are presented on Fig. 3.1. This are Elasto-Plastic models with hardening in the regular part and softening on the singular part. For the concrete, since the behavior is non symmetric, we use two independent displacement jumps, α_t^i in tension and α_c^i in compression.

From the stresses in each fiber, we compute the stress resultants in the cross sections

$$N = \int_S \sigma_x dS;\; V = \int_S \sigma_{xy} dS;\; M = -\int_S y^2 \sigma_x dS \tag{18}$$

The solution procedure in, in the same manner as in Eqs. (12) and (14), split into local resolutions on each fiber and a global resolution with a modified stiffness matrix obtained by static condensation.

3.2 Combined axial load and bending moment threshold functions

Since we want to use the macro stress resultant model presented in section 2 to compute the response of reinforced concrete frames, we must take into account the interaction between axial force and bending moment (especially for columns). Thus, the threshold functions of Eq. (15) are rewritten as

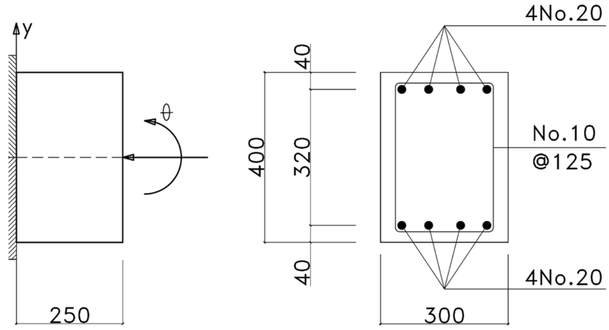

Fig. 5 Geometry of reinforced concrete beam-column for parameter identification

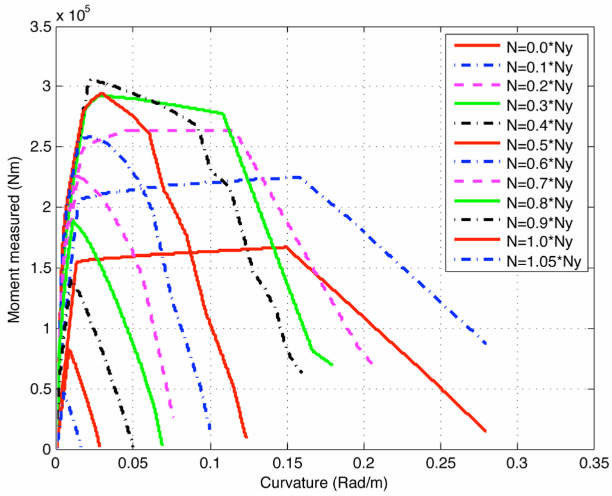

Fig. 6 Moment-curvature relations obtained by multi-fiber beam-column model

$$\Phi^M(M,N,\zeta_i^M):=|M|-(M_i(N)+K_i(N)I\cdot\zeta_i^M)\leq 0 \tag{19}$$

We present the procedure of identification of the parameter on a particular example of reinforced concrete beam-column frame element (Fig. 5). The dimensions of rectangular cross-section of the beam are $b\times h$ equal to 30×40 (cm). Inside the cross-section, four rebars of diameter 20 mm are placed at the top and the bottom. The concrete has compressive strength f_c'=30 MPa, tensile strength f_{ct}=1.8 MPa, modulus of elasticity E_b=28,600 MPa. By using the multi-fiber model for parameter identification, we use the divided rectangular cross-section of the beam with 20 concrete layers and 8 discrete fibers for describing the steel reinforcements.

In the first step, we compute the limit values of axial force for this beam without bending moment by imposing only an axial displacement. We obtain the yield axial force N_y. Then, for different ration of axial force $n=N/N_y$, we compute the bending moment-curvature response while imposing N constant and increasing rotation of the right end of the element. The responses for 12 different ratios are presented on Fig 6. We can separate these diagrams into two main groups: the first one for axial force ratios n from 0 to 0.4 and the second for axial force ratios n from 0.4 to 1.05. The first group corresponds to the large-eccentricity cases, where the failure in the reinforced-concrete beam is

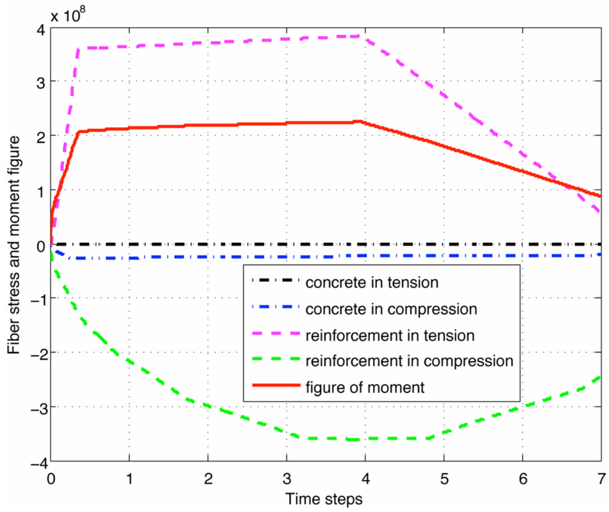

Fig. 7 Fiber stress-time curves and moment-time curve

induced by the yielding of reinforcement in tension zone. With the increasing values of axial force we can obtain the corresponding increase in values of cracking, yielding and ultimate moment (M_c, M_y, M_u), where the values of M_y and M_u will differ clearly. We also have fairly long part with hardening response diffuse of plastic phase. The second group corresponds to the small-eccentricity case, where the failure process is governed by the compressive failure of concrete in compression zone. With the increase of axial force, we obtain a small difference between the values of yield and ultimate moments, and the value of ultimate moment can even become smaller than the yield moment ($M_u \leq M_y$).

In order to determine the parameters for the stress resultant model, namely the cracking, yielding, and ultimate moments (M_c, M_y, M_u) and the corresponding curvature values, we present the stress-time curves for four particular fibers are chosen in the cross-section: two for the reinforcements, one in tension zone and the other in compression zone, and two for the concrete, one is tension and one in compression, at the top and bottom edges of the cross-section where the strain values are the largest. For those selected fibers, we can identify easily all limitations for moment following the limit stresses of concrete and steel fibers. The crack-moment M_c corresponds to the the tensile cracking of the bottom concrete fiber. The yield-moment M_y is reached when the tensile steel fiber reaches its yield strength f_y. For the large-eccentricity in compression case, the ultimate moment M_u is equal to the maximum value of moment M_{max} for each types of cross-section. But for small-eccentricity compression case, M_u is identified from the change of tangent modulus, namely, the point where the tangent modulus changes suddenly from the plastic phase to the softening phase. For these three particular points, we can have the corresponding curvatures, κ_c, κ_y and κ_u. The ultimate state (no more load capacity), (M_t, κ_t) is assumed to be the the point where the compressive concrete fiber at the same position of the compressive steel fiber is damaged completely. From this point we can deduce the last point of the macro model (M=0, κ_p), by extrapolation of the softening phase until M=0.

The limit bending moments for different ratios of compressive force are represented on Fig. 8(a). We recognize clearly the previously defined expression distinguishing two eccentricity compression

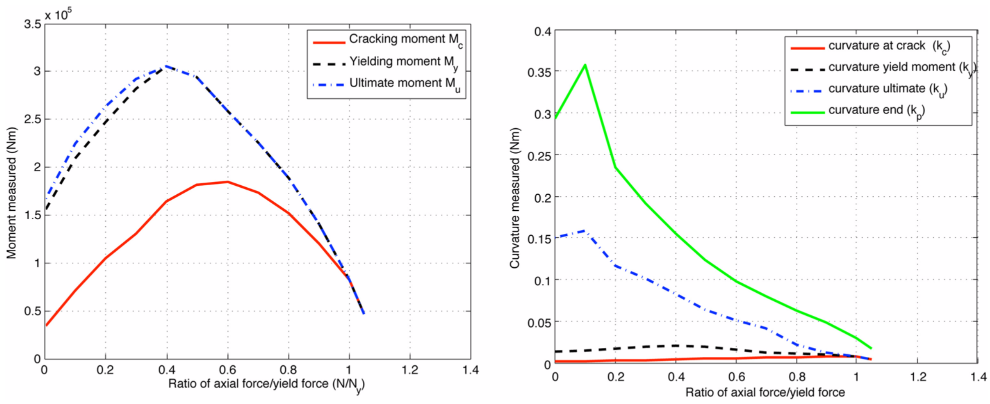

Fig. 8 Variation of parameters with respect to N/Ny ratio: (a) Bending moments, (b) Curvatures

cases. For $n=N/N_y$ varying from 0 to 0.4, the values of yield and ultimate moments increase. In the opposite, for larger values of n varying from 0.4 to 1.05, the values of yield and ultimate moments decrease. The variations of M_y and M_u are quite similar, while for the cracking moment M_c, the changing tendency is for a value of n equal to 0.6.

The limit curvatures for different ratios of compressive force are represented on Fig. 8(b). We note that the curve shapes of curvature κ_u and κ_p are different from those of curvature κ_c and κ_y. The curves of κ_u and κ_p increase linearly for values of n between 0 and 0.1, and decrease for larger values of n. The curve of κ_c always increases linearly, while the curve of κ_y reaches its maximum for a value of n equal to 0.4.

From this step, we can use directly the computed values of the limit bending moments and corresponding curvatures from Fig. 8 to introduce them in the threshold functions of Eq. (19). The values of tangent modulus can be computed with

$$
\begin{aligned}
K_1(n) &= (M_y(n) - M_c(n))/(\kappa_y(n) - \kappa_c(n)) \\
K_2(n) &= (M_u(n) - M_y(n))/(\kappa_u(n) - \kappa_y(n)) \\
K_3(n) &= (M_p(n) - M_u(n))/(\kappa_p(n) - \kappa_u(n))
\end{aligned}
\tag{20}
$$

For values of n between two computed points, we can make a linear interpolation. An other possibility is to find the best-fit polynomial interpolation of the different curves of Fig. 8 with an optimization tool. It has been done in Pham (2009).

Since the identification procedure presented in this section is done with computations on a single multi-fiber beam finite element, it is very fast. The computation of the whole reinforced concrete frame structure will now be very fast done with the stress resultant beam elements. In the next section, we present different examples to show the precision and the robustness of the method.

4. Numerical examples

4.1 Single element with variation of axial force

The threshold functions of the macro element have been identified for different levels of axial

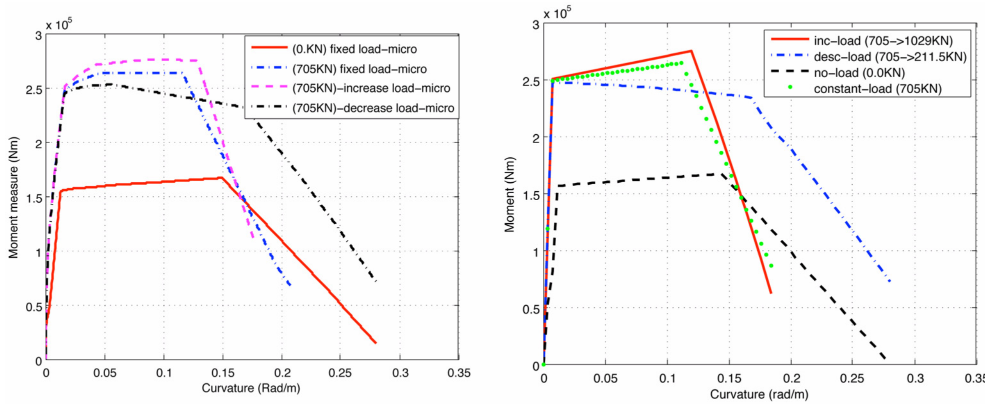

Fig. 9 Single element with variation of axial force during rotation loading: (a) Multi-fiber element, (b) Macro-element

force. But for each level, the axial force remained constant during the computation (only the rotation and the bending moment changed). In a real structure, between two time step, the axial force can change, and thus the threshold functions change (the axial force is considered as a local variable in the threshold functions). This could lead to numerical problems.

The first numerical example is to test the robustness in case of variation of axial force. It is the same element used in the section 3.2. (Figs. 3(b) and 5), but in this case, the axial force varies with the time. Four cases of loading program have been computed. For the first one $N = 0$, for the second one $N = 705$ kN, for the third one N increased from 705 kN to 1029 kN and for the last one N decreased from 705 kN to 211.5 kN. Fore each case, the computation was done first with the multi-fiber element of section 3.1 to have a reference. The second computation was done with the procedure presented in this paper (identification of the threshold functions with constant axial forces and then computation with the macro stress resultant element).

The results are presented on Fig. 9. We can see that the results of the macro model (right) are very close to those of the multi-fiber model (left). They are only more sharp since there is no progressive yielding of the fiber, one after the other. On the other hand, the cost used for computation with the macro model is much smaller than the one for computation with multi-fiber model.

4.2 Two storeys reinforced concrete frame

In the second numerical example, we consider a reinforced-concrete frame with two floors and one span. The dimensions of the frame are detailed in the Fig. 10. The cross-section of both column and beam is $b \times d = 30 \times 40$ (cm). In both beam and column, $4\phi20$ mm of the longitudinal bar are placed at each side, and the stirrups $\phi10$ mm at the distance $a = 125$ mm are used along to the length of span and the height of two-storey. This example is based on the experiment presented in (Vecchio and Emara 1992). Two fixed vertical forces $P = 700$ KN are applied at two nodes on the top of the frame representing the effect of the dead load. The lateral force is imposed on one side at the top node with the values increasing from zero to the time of the complete collapse of the frame.

The finite element model used in the numerical computations is as follows: each column with the height $h = 2$ m is divided into 8 elements with $L_e = 0.25$ m and each beam with the length $L = 3.5$ m

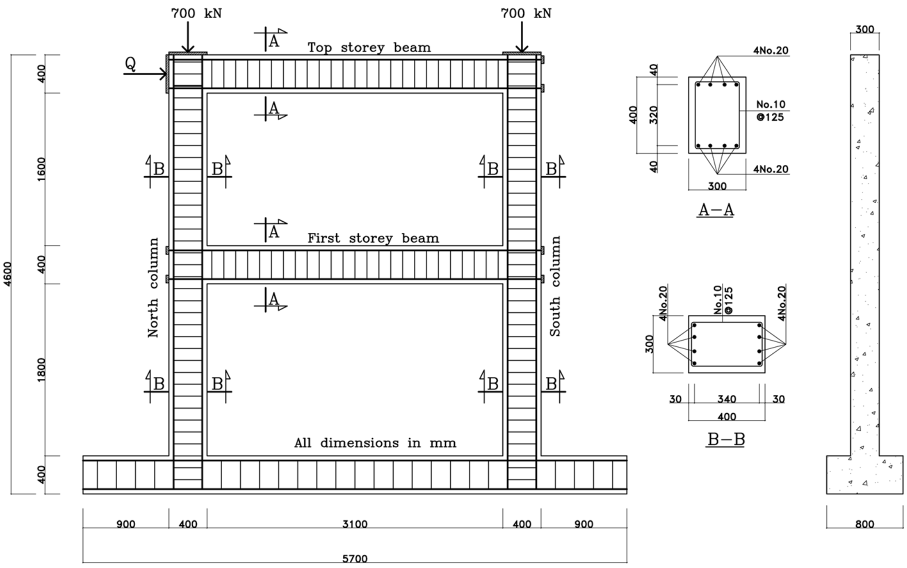

Fig. 10 RC frame experiment

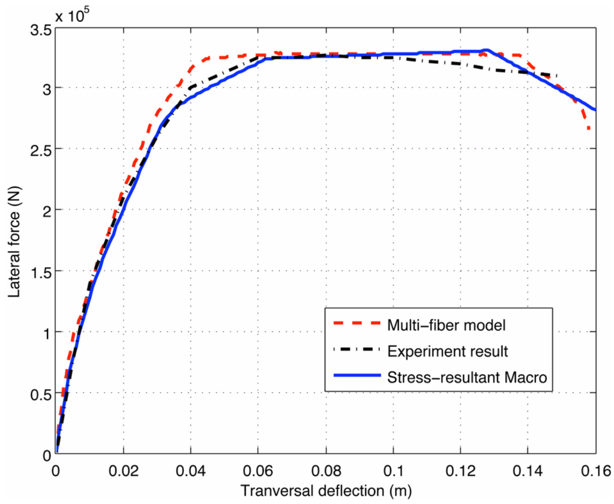

Fig. 11 Order of appearence of failure hinges: (a) Constant axial load threshold, (b) Varying axial load threshold

is divided into 14 elements with $L_e = 0.25$ m. The concrete has compressive strength $f_c' = 30$ MPa, tensile strength $f_{ct} = 1.8$ MPa, modulus of elasticity $E_b = 28{,}600$ MPa. All the details on material parameters and geometry for the test can be found in Vecchio and Emara (1992).

The cross section dimensions are the same as the one used in section 3, we thus use the same threshold functions for the stress resultant macro element. Like in the first example (section 4.1), we compare the response obtained with the macro elements and the procedure described in this paper to the reference obtained with a complete multi-fiber elements computation. Both are also compared to the test result on Fig. 11. The three curves are close together. The curve with the stress resultant macro model is very fast to compute.

We can note that, thanks to the good modeling of the softening branches in our models, both multi-fiber model and macro model can catch the failure and descending branch of the frame response. This is not the case with usual softening stress strain models where numerical difficulties appear when reaching this failure.

We tried to compute the response of the frame without taking into account the variation of axial force in the elements (Pham 2009). A constant axial load of 0 kN and 700 kN was used to identify the threshold functions respectively of the beams and of the columns. It didn't change a lot the global response, but the appearance of plastic and failure hinges was very different from the case where the axial force varies in the threshold functions used in the computation. Thus it is important to take into account this variation.

5. Conclusions

We presented a stress resultant beam macro model to compute the response of reinforced concrete frames. This model is consistent until the failure due to the softening response of the elements. It can be use for the performance-based design statically indeterminate structures where the failure of one single element does not always lead to the complete failure of the structure. The procedure, from the identifications of the macro model parameters, until the complete computation of the structure is very fast, thus we can seek to optimize a number of factors that are involved in the computed nonlinear response, such as material properties of concrete and steel, the dimensions of the cross-section, the steel reinforcement ratio. This is made possible for any particular loading program by the approach presented herein, which relies on material level information (with the realistic properties of concrete and steel, including the localized failure) in order to build the stress resultant model for a particular reinforced concrete cross-section. In this manner we end up with what is most likely the most reliable basis for parameter identification which possesses the predictive capabilities. Moreover, the idea to build the stress-resultant constitutive model for a RC beam from the corresponding properties of the constituents is the main advantage with respect to classical and more recent works on ultimate limit load failure of frame structure, where the stress-resultant models are proposed in a fairly ad-hoc manner.

References

Abrams, D.P. (1987), “Influence of axial force variations on exural behavior of reinforced concrete columns”, *ACI Struct. J.*, May-June.

Anthoine, A., Guedes, J. and Pegon, P. (1997), “Non-linear behavior of reinforced concrete beams: from 3D continuum to 1D member modeling”, *Comput. Struct.*, **65**(6), 949-963.

Armero, F. and Ehrlich, D. (2006), “Numerical modeling of softening hinges in thin euler-bernoulli beams”, *Comput. Struct.,* **84**, 641-656.

Asferg, J.L., Poulsen, P.N. and Nielsen, L.O. (2007), “A direct XFEM formulation for modeling of cohesive crack growth in concrete”, *Comput. Concrete*, **4**(2), 83-100.

Cipollina, A., Lopez-Inojosa, A. and Florez-Lopez, J. (1995), “A simplified damage mechanics approach to nonlinear analysis of frames”, *Comput. Struct.*, **54**, 1113-1126.

Dufour, F., Pijaudier-Cabot, G., Choinska, M. and Huerta, A. (2008), “Extraction of a crack opening from a continuous approach using regularized damage models”, *Comput. Concrete*, **5**(4), 375-388.

Ehrlich, D. and Armero, F. (2005), “Finite element methods for the analysis of softening plastic hinges in beam and frames", *Comput. Mech.*, **35**, 237-264.

EURO CODE 2, *Design of concrete structures - Part 1-1 : general rules and rules for buildings*.

Florez-Lopez, J. (1998), "Frame analysis and continuum damage mechanics", *Eur. J. Mech. - A/Solids*, **17**(2), 269-283.

Ibrahimbegovic, A. and Wilson, E. (1991), "A modified method of incompatible modes", *Commun. Numer. Meth. Eng.*, **7**, 187-194.

Ibrahimbegovic, A. (2009), *Nonlinear solid mechanics - theoretical formulations and finite element solution methods*, Springer, 576.

Ibrahimbegovic, A. and Brancherie, D. (2003), "Combined hardening and softening constitutive model of plasticity: precursor to shear slip line failure", *Comput. Mech.,* **31**, 88-100.

Ibrahimbegovic, A. and Frey F. (1993), "Stress resultants finite element analysis of reinforced concrete plates", *Eng. Comput.*, 15-30.

Ibrahimbegovic, A. and Frey, F. (1993), "An efficient implementation of stress resultant plasticity in analysis of reissner-mindlin plates", *Int. J. Numer. Method. Eng.*, **36**, 303-320.

Jirasek, M. (1997), "Analytical and numerical solutions for frames with softening hinges", *J. Eng. Mech. - ASCE,* **123**(1), 8-14.

Marante, M.E. and Florez-Lopez, J. (2003), "Three-dimensional analysis of reinforced concrete frames based on lumped damage mechanics", *Int. J. Solids Struct.*, **40**, 5109-5123.

Marante, M.E., Picon, R. and Florez-Lopez, J. (2004), "Analysis of localization in frame members with plastic hinges", *Int. J. Solids Struct.,* **41**, 3961-3975.

Nanakorn, P. (2004), "Two-dimensional a beam-colum finite element with embedded rotational discontinuities", *Comput. Struct.*, **82**, 753-762.

Pham, B.H. (2009), *Stress resultant model for optimal design of reinforced concrete frames*, PhD Thesis, Ecole Normale Superieure de Cachan, France.

Rajasankar, F.J., Nagesh, R.I. and Meher, A. (2009), "Prasad Modelling inelastic hinges using CDM for non linear analysis of reinforced concrete frame structures", *Comput. Concrete*, **6**(4), 319-341.

Vecchio, F.J. and Emara, M.B. (1992), "Shear deformations in reinforced concrete frames", *ACI Struct. J.,* **89**(1), 46-56.

Zingales, M. and Elishako, I. (2000), "Localization of the bending response in presence of axial load", *Int. J. Solids Struct.* **37**, 6739-6753.